DAMAGE-CONTROLLED STRUCTURES. I: PRELIMINARY DESIGN METHODOLOGY FOR SEISMICALLY ACTIVE REGIONS

By J. J. Connor,[1] Fellow, ASCE, A. Wada,[2] Member, ASCE, M. Iwata,[3] and Y. H. Huang[4]

ABSTRACT: A damage-controlled structure is defined as a combination of structural systems and energy transformation devices that are integrated in such a way that damage due to a major loading is restricted to a specific set of elements that can be readily repaired. This paper describes a preliminary design methodology for building structures subjected to seismic loading, and presents a comprehensive set of numerical simulations illustrating the response of typical structures designed according to this methodology. The proposed design considers the structure to consist of two independent structural systems that work together to satisfy a design requirement on the deformation. The first system functions as the principal load-carrying mechanism for vertical and lateral service loads, while the second structure's role is to dissipate and absorb the energy introduced by significant ground shaking. The key design parameters are the elastic stiffness distribution of the primary system, and the damping characteristics of the secondary system. An optimal evaluation of these parameters is presented for a specific choice of material strengths. The data show that the damage control design paradigm generates very good estimates for preliminary design in this case.

INTRODUCTION

A damage-controlled structure is defined as a combination of several structural systems and energy transformation devices that are integrated in such a way as to restrict damage to a specific set of structural elements that can be readily repaired. In conventional structural design the stiffness and absorption mechanisms are combined in a single system, and the structure is allowed to deform inelastically. Experience with recent earthquakes has shown that the economic penalty associated with repairing conventionally designed structures can be significant. This issue is the motivation for the present design approach. The potential benefit of damage control is illustrated in Fig. 1 which shows the relationship between repair cost and level of earthquake intensity for conventional and damage controlled designs (Iwata 1994). It indicates that a damage controlled structure is most effective for moderately large excitations.

Since damage is due to structural motion, damage control is achieved through the control of structural motion. The motion control strategy described in this paper is based on the approach advanced by Connor and Wada (1992), and later applied by Iwata et al. (1992). They argue that the spatial distribution of motion depends mainly on the structural stiffness, whereas the amplitude of motion is governed by both the stiffness and energy dissipation/absorption of the structure. Therefore, they propose using a two-step procedure: (1) establish the stiffness distribution that produces the desired spatial variation of displacement; and (2) integrate energy dissipation and absorption mechanisms with the structural system to adjust the magnitude of the response.

The design approach adopted here is based on employing two independent structural systems: (1) a primary system that supports the vertical loading and also provides the lateral stiffness; and (2) a bracing system that functions as the energy dissipation/absorption mechanism for lateral loading. Fig. 2 illustrates this concept for a building. In the case of a major seismic event, the primary system is required to behave elastically, whereas the bracing system is allowed to experience substantial inelastic deformation while remaining stable (no buckling allowed) and accessible for repair.

The effectiveness of this structural concept depends on the energy dissipation capacity of the braces and on the ability of the primary structure to remain elastic during the motion associated with a major seismic event. These requirements necessitate the use of very-high–strength material for the primary structure and very low strength material for the bracing system. The second part of this paper describes an experimental study of typical structural panels for a set of steel structures. Steel strengths ranging up to 800 MPa for the primary structure and as low as 100 MPa for the braces were considered. The experimental results confirm the technical feasibility of this design concept. Additional design optimization studies are reported in Huang and Wada (1993).

DESIGN APPROACH

The design of a damage-controlled building for seismic excitation involves specifying the input energy of the earthquake, establishing the distribution of lateral stiffness in the primary structure, and defining the magnitude and variation of the hysteretic damper (HD) parameters, such as yield force, over the height of the building. Akiyama's concept of equivalent ve-

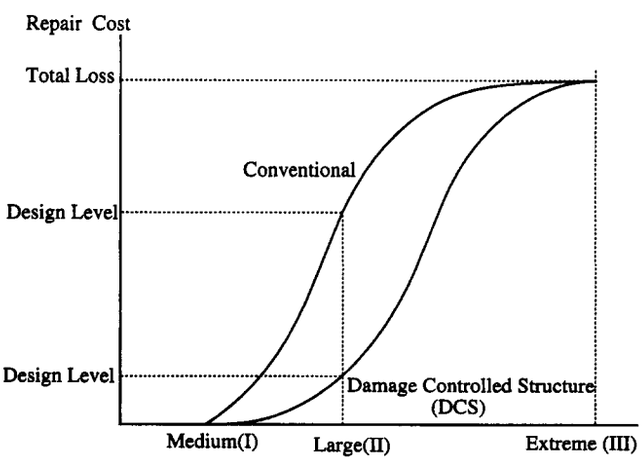

FIG. 1. Repair Cost versus Earthquake Intensity

[1]Prof. of Civ. and Envir. Engrg., Massachusetts Inst. of Technol., Cambridge, MA 02139.

[2]Prof. of Struct. Engrg., Res. Lab. of Engrg. Mat., Tokyo Inst. of Technol., Nagatsuta 4259, Midori, Yokohama 227, Japan.

[3]General Mgr. of Build. Constr. Div., Nippon Steel Corporation, Otemachi 2-6-3, Chiyoda-ku, Tokyo 100, Japan.

[4]Asst. Prof. of Struct. Engrg., Res. Lab. of Engrg. Mat., Tokyo Inst. of Technol., Nagatsuta 4259, Midori, Yokohama 227, Japan.

Note. Associate Editor: Nicholas P. Jones. Discussion open until September 1, 1997. To extend the closing date one month, a written request must be filed with the ASCE Manager of Journals. The manuscript for this paper was submitted for review and possible publication on September 27, 1994. This paper is part of the ***Journal of Structural Engineering***, Vol. 123, No. 4, April, 1997. ©ASCE, ISSN 0733-9445/97/0004-0423–0431/$4.00 + $.50 per page. Paper No. 9349.

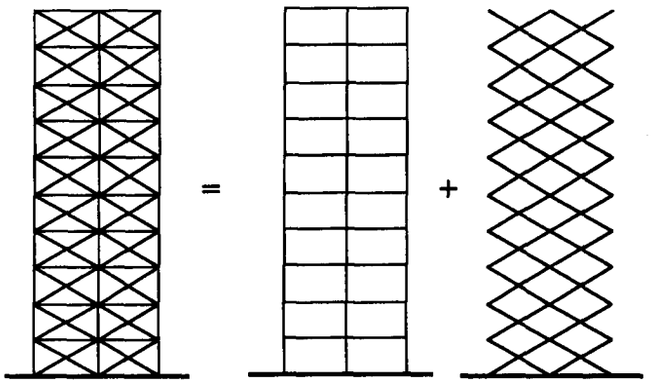

FIG. 2. Concept of Damage-Controlled Building Structure (DCS): (a) Actual Structure; (b) Primary Structure; (c) Brace System

locity (Akiyama 1985), is used to establish the seismic energy input and scale the accelerograms used in the numerical simulations. The determination of the optimal lateral stiffness distribution is based on the procedure introduced in Connor and Wada (1992), and applied in Wada and Huang (1993), and Connor and Klink (1994). A similar approach is followed to establish the HD properties.

In what follows, the derivation of the optimal structural stiffness and HD yield force distributions is described. Then, the behavior of a typical structure is illustrated through numerical simulations carried out on a simplified lumped parameter model. Guidelines for selecting the HD yield force distribution for seismic loading are proposed for a limited range of structures. Additional work to extend these guidelines to a broader range of structures, and incorporate other types of energy dissipation mechanisms is ongoing.

OPTIMUM STIFFNESS DISTRIBUTION

Structural Models

The primary structural system composed of beams and columns is modeled as an equivalent beam having variable transverse shear (D_T) and bending (D_B) rigidities. The corresponding deformation measures are denoted by γ (shear) and κ (bending). A design is considered to be optimal when γ and κ are essentially uniform over the building height, and their maximum values are below the specified limits. Given D_T and D_B, one can determine the required properties for the structural elements composing the beam cross section; the focus of this analysis is therefore on how to evaluate D_T and D_B.

Fig. 3 shows the deformed configuration of the hysteretic damper-brace system and defines the relevant notation. The dampers are considered to be elastic-perfectly plastic elements with a yield force level F_y. Superimposing the contributions of adjacent braces and taking the transverse shear deformation as the motion measure leads to the relationship shown in Fig. 3(c). The relevant equations are

$$Q = 2F\cos\alpha;\quad e = \delta\cos\alpha;\quad \gamma = \delta/h;\quad k_D = 2kh\cos^2\alpha \qquad (1a\text{–}d)$$

Numerical simulations are carried out using the lumped parameter model shown in Fig. 4. Hysteretic damping due to the braces is modeled with bilinear springs and the derivation of the lumped parameter properties is based on energy equivalence. More sophisticated models, such as a finite-element beam model, were not considered here since experience (Tajimi 1965) has shown that simplified models are adequate for preliminary design comparison studies.

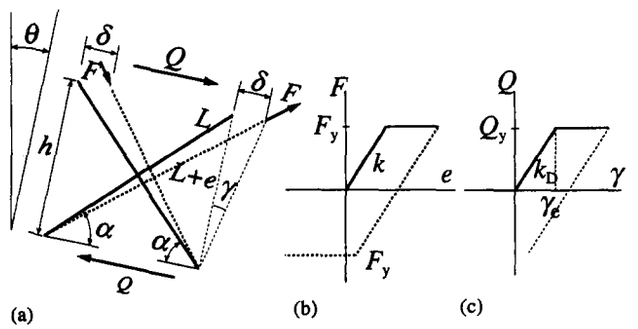

FIG. 3. Definition of Hysteric Damper—Brace System: Brace Deformation; (b) Individual Brace System; (c) Brace Response System

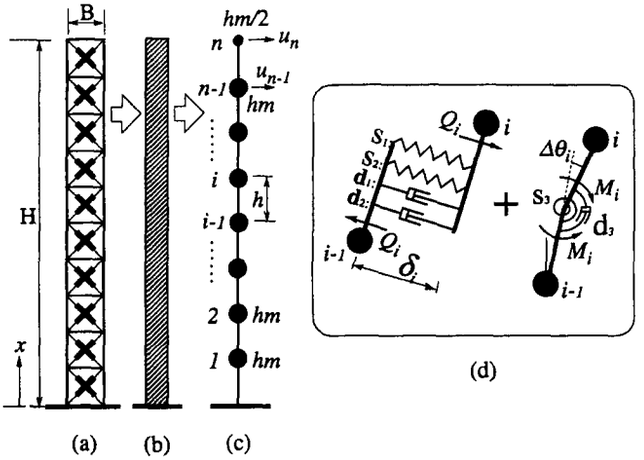

FIG. 4. Lumped Parameter Model

Initial Stiffness Distribution

The goal is to achieve uniform shear and bending deformation over the height of the structure during seismic excitation. Since the response is dynamic, a logical starting point is to postulate the stiffness distribution such that the first mode shape has those characteristics. The appropriate distributions are (Connor and Wada 1992)

$$D_T = \frac{Q}{\gamma} = \frac{m\omega_1^2 H^2}{2}\left(1+\frac{A}{3}\right)\tilde{D}_T \qquad (2a)$$

$$D_B = \frac{M}{\kappa} = \frac{m\omega_1^2 H^4}{2}\left(\frac{1}{4}+\frac{2}{3A}\right)\tilde{D}_B \qquad (2b)$$

$$\tilde{D}_T = \alpha_0 + \alpha_1\bar{x} + \alpha_2\bar{x}^2 + \alpha_3\bar{x}^3 \qquad (2c)$$

$$\tilde{D}_B = \beta_0 + \beta_1\bar{x} + \beta_2\bar{x}^2 + \beta_3\bar{x}^3 + \beta_4\bar{x}^4 \qquad (2d)$$

where H = total building height; B = width of building; $\bar{x}$ = relative height ($=x/H$); f = ratio of specified shear to column strains; A = dimensionless parameter ($=2H/fB$); m = mass per unit height; ω_1 = fundamental frequency of structure in radians; α_i, β_i = stiffness distribution coefficients that depend only on parameter A. Their values are listed in the first column of Table 1.

Considering only the first mode, the base shear can be expressed as (Connor and Klink 1994)

$$Q(0) = \omega_1\Gamma_1 S_v(\omega_i,\xi_i)\frac{mH}{2}\left(1+\frac{A}{3}\right) \qquad (3a)$$

$$\Gamma_1 = \frac{1+A/3}{2/3+A/2+A^2/10} \qquad (3b)$$

TABLE 1. Stiffness Distribution Coefficients

Coefficient (1)	Based on first mode (2)	Corrected for higher modes (3)
α_0	1	$1.1412 + 0.1812A$
α_1	0	$-0.4737 - 0.6512A + 0.1156A^2$
α_2	$3/(3 + 2A)$	$-0.0422 + 0.9980A - 0.3332A^2$
α_3	$2A/(3 + 2A)$	$-0.4338 - 0.4026A + 0.2132A^2$
β_0	1	$1.1034 - 0.0122A + 0.0088A^2$
β_1	$2(3 + 2A)/(3A + 4)$	$-1.6279 - 0.0830A - 0.0088A^2$
β_2	0	$0.5408 + 0.7688A - 0.1924A^2$
β_3	$2/(3A + 4)$	$-0.3113 - 1.0494A + 0.3696A^2$
β_4	$A/(3A + 4)$	$0.2971 + 0.3728A - 0.1768A^2$

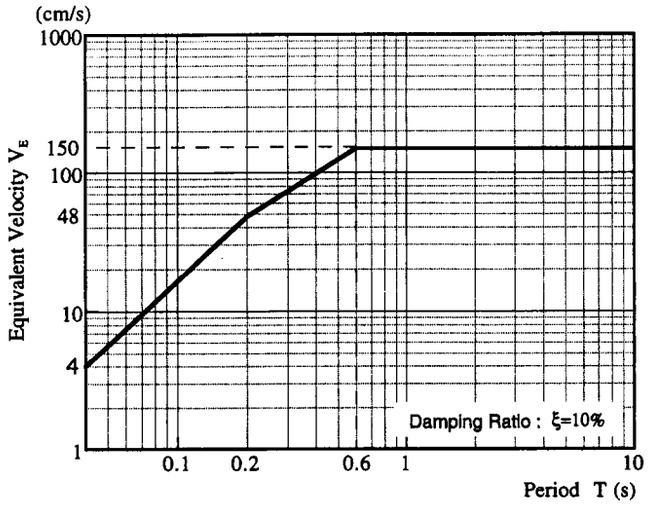

FIG. 5. Equivalent Velocity Response Spectrum

where Γ_1 = participation factor; ξ_1 = damping ratio; and $S_v(\omega_1, \xi_1)$ = pseudospectral velocity. The expression proposed by Akiyama (1985) is used to relate S_v to the equivalent velocity V_E

$$S_v(\omega_i, \xi_i) = \frac{V_E(\omega_i, \xi_i)}{1 + 3\xi_i + 1.2\sqrt{\xi_i}}; \quad \xi_i = \xi_i \frac{\omega_i}{\omega_1} \tag{4a,b}$$

Defining γ^* as the desired shear deformation for a given level of seismic excitation, V_E, and substituting for Q, γ in (2) evaluated at $\bar{x} = 0$, results in the following estimate for ω_1:

$$\omega_1 = \frac{\Gamma_1 S_v(\omega_1, \xi_1)}{H\gamma^*} = \frac{2\pi}{T_1} \tag{5}$$

The equivalent velocity design spectrum used in this study is shown in Fig. 5 (AIJ 1993). For $T > 0.60$; V_E and S_v are constant; and (5) leads directly to ω_1, i.e., no iteration is required. Finally, using (5), the stiffness distributions specialized for seismic excitation take the following form:

$$D_T = \tilde{D}_T \tilde{D}_T, \quad \tilde{D}_T = \frac{m}{2}\left(1 + \frac{A}{3}\right)\left[\frac{S_v\Gamma_1}{\gamma^*}\right]^2 \tag{6a}$$

$$D_B = \tilde{D}_B \tilde{D}_B, \quad \tilde{D}_B = \frac{mH^2}{2}\left(\frac{1}{4} + \frac{2}{3A}\right)\left[\frac{S_v\Gamma_1}{\gamma^*}\right]^2 \tag{6b}$$

where $\tilde{D}_T$, $\tilde{D}_B$ are defined in (2).

Corrected Stiffness Distribution

Numerical simulations for earthquake excitation applied to reasonably tall buildings show that (2) underestimates the stiffness in the lower and upper regions. Since (2) is based on only the first mode, these results indicate that the influence of the higher modes needs to be incorporated in the stiffness distribution. The correction procedure employed here modifies the expressions for α_i, β_i by (1) using numerical simulation to generate the response for a broad range of the structural parameters; and (2) applying the least-squares method to derive polynomial approximations for the stiffness coefficients. Although this calibration is based on seismic excitation, it can be readily modified for other loading types.

The procedure is as follows. For a given excitation level, structural response parameters are calculated, taking into account higher modes, for a building whose characteristics are identified by the parameter A. The shear and bending deformation distributions are evaluated using the initial stiffness profile and the calculated maximum force and moment responses. Subsequently, $\tilde{D}_T$ and $\tilde{D}_B$, which represent the initial stiffness distributions, are modified according to the ratio of initial to target deformations

$$\tilde{D}_T|_{\text{modified}} = \frac{\gamma}{\gamma^*}\tilde{D}_T|_{\text{initial}}; \quad \tilde{D}_B|_{\text{modified}} = \frac{\varepsilon}{\varepsilon^*}\tilde{D}_B|_{\text{initial}} \tag{7a,b}$$

$$\varepsilon = \frac{B}{2}\kappa; \quad \varepsilon^* = \frac{\gamma^*}{f} \tag{7c,d}$$

Estimates of α_i and β_i for a given A are obtained by using the method of least squares to fit the modified stiffness distributions with the polynomial expansions for $\tilde{D}_T$, $\tilde{D}_B$ defined in (2). The process is repeated for a large number of buildings with varying characteristics identified by the parameter A. Finally, the method of least squares is applied again to generate polynomial expansions for α_i, β_i in terms of A.

According to this derivation, $\tilde{D}_T$ and $\tilde{D}_B$ are independent of the target deformation γ^* and depend only on A. Simulations show essentially no change in $\tilde{D}_T$ and $\tilde{D}_B$ for a five-fold change in γ^* with A held constant. The variation of the stiffness distribution with A is illustrated in Fig. 6. The maximum percentage change in stiffness occurs in the upper regions and is of the order of 100%; near the base, the correction is only in the range of 20%.

Fifty-four sample buildings were considered, together with three values for γ^*; 1/100, 1/200, 1/400. Table 2 lists the corresponding values of A used in the numerical simulation. The final expressions for the stiffness coefficients, $\tilde{D}_T$ and $\tilde{D}_B$, derived with the least-squares method are listed in the column 3 of Table 1. An alternate numerical approach to modify the stiffness distribution is described in Connor and Klink (1994).

Studies show that the distributions based on (6) and the semiempirical expressions listed in Table 1 are adequate for preliminary design. However, (5) tends to overestimate the fundamental period since it is based on the initial, unmodified stiffness. An improved estimate of the period, generated by

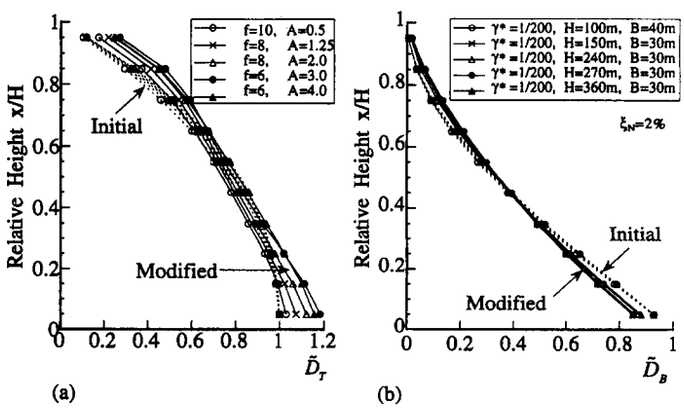

FIG. 6. Variation of Stiffness Distribution with A: (a) Shear Stiffness Distribution; (b) Bending Stiffness Distribution

TABLE 2. Values of A for Building Case Studies

H (m) (1)	f (2)	B (m) 20 (3)	30 (4)	40 (5)	50 (6)	80 (7)	100 (8)
150	6	2.5	1.67	1.25	1.0	0.625	0.5
150	12	1.25	0.833	0.625	0.5	0.312	0.25
150	18	0.833	0.556	0.417	0.333	0.208	0.167
200	6	3.333	2.222	1.67	1.333	0.833	0.667
200	12	1.667	1.111	0.833	0.667	0.417	0.333
200	18	1.111	0.74	0.556	0.444	0.278	0.222
250	6	4.167	2.778	2.083	1.667	1.042	0.833
250	12	2.083	1.389	1.042	0.833	0.521	0.417
250	18	1.389	0.926	0.694	0.556	0.347	0.278

Note: $A = 2H/fB$.

applying the iterative scheme to the sample buildings, is given by Huang (1994).

$$T_1 = 0.932 \frac{2\pi H \gamma^*}{\Gamma_1 S_v(\xi_1, \omega_1)} \tag{8}$$

Eq. (8) is appropriate for $T_1 > 0.6$.

Numerical Comparisons

Results illustrating the performance of a typical tall building having the proposed optimum stiffness distribution and building properties are presented in this section. Note that $f = 8$ corresponds to allowing the transverse shear strain to be eight times the column strain. The properties of the example building are as follows:

H = 200 m
B = 40 m
m = 10,000 kg/m
S_v = 1.22 m/s
f = 8
γ^* = 1/200
ξN = 2%.

Fig. 7 shows stiffness distributions based on the first mode (original) and higher modes (modified). The fundamental periods corresponding to both stiffness distributions are determined according to (5) and (8). The equivalent velocity spectrum used is shown in Fig. 5. It appears that the contribution of the higher modes is relatively more dominant for shear than for bending.

Fig. 8 shows the shear and bending deformation profiles for the example building; the response results are obtained with the SRSS method. Curve (A) in Fig. 8 defines the target deformation γ^*; (B) is the profile when only the first mode is considered; (C) is the profile corresponding to the original stiffness; and (D) denotes the result obtained with the modified stiffness. The improvement in the deformation profile near the top of the building is sufficient for preliminary design.

DISTRIBUTED HYSTERETIC DAMPING

The bracing system at a particular location, x, can be represented by a single "equivalent" shear damper as illustrated in Fig. 3. For design, the yield force level Q_y and the elastic limit γ_e need to be specified. One starts by specifying the material properties (σ_y^b, ε_y^b) for the brace, leading to the design value for γ_e

$$\gamma_e = \varepsilon_y^b \left(\frac{2}{\sin 2\alpha} \right) \tag{9}$$

and a relationship between Q_y and the required brace cross-sectional area A_b

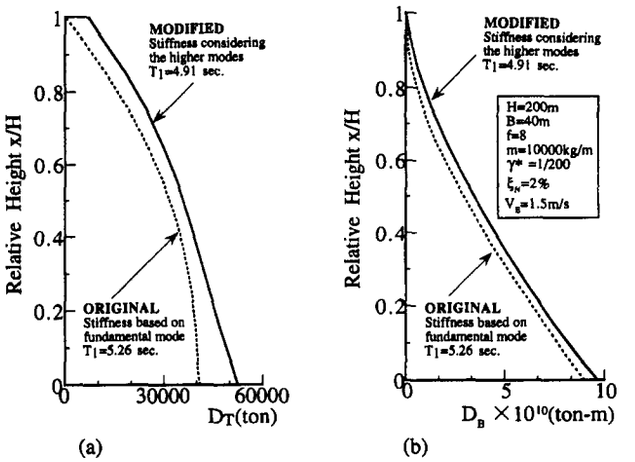

FIG. 7. Dimensionless Stiffness Distributions—Example Buildings: (a) Shear Stiffness; (b) Bending Stiffness

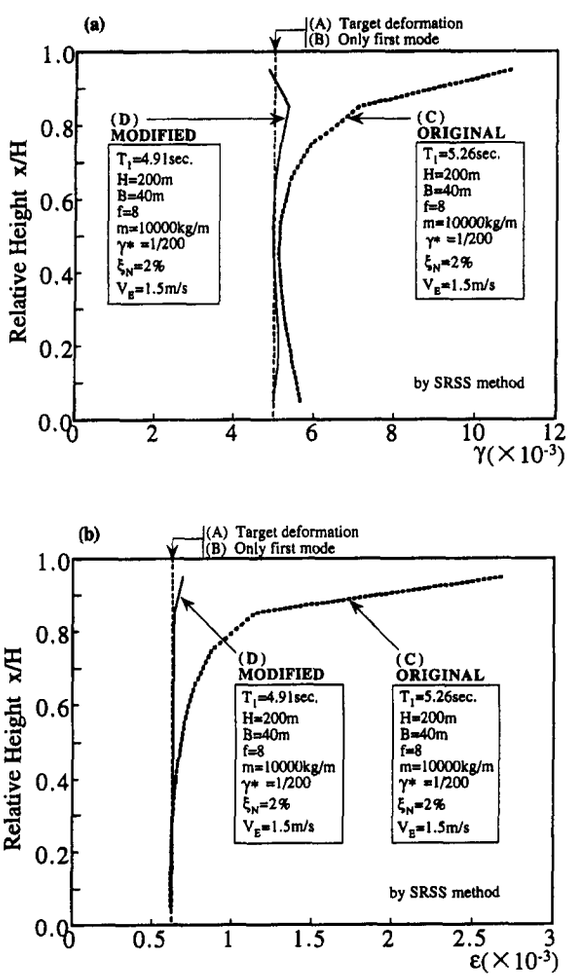

FIG. 8. Comparison of Deformation Response—Example Building: (a) Shear Deformation; (b) Bending Deformation

$$Q_y = \sigma_y^b (\cos \alpha) n_b A_b \tag{10}$$

where n_b = number of brace elements at that location. Therefore, the problem reduces to specifying the variation of Q_y over the building height. To resolve this issue, one needs to consider the hysteretic energy dissipation for one brace and relate it to the total energy dissipation requirement as measured by the equivalent velocity V_E.

Our strategy is to represent hysteretic damping as "equivalent" viscous damping because it is easier to deal with ana-

lytically and familiar to design engineers. Considering periodic excitation, the energy per unit height dissipated in a single cycle through hysteretic damping is given by

$$\gamma = \bar{\gamma} e^{i\omega t}; \quad E_{HD} = 4Q_y(\bar{\gamma} - \gamma_e) \tag{11a,b}$$

Defining C_H as the equivalent distributed viscous damping parameter, and equating the energy dissipation terms leads to

$$Q = C_H \frac{\partial \gamma}{\partial t}; \quad C_H = \frac{4Q_y}{\pi\omega\bar{\gamma}}\left(\frac{\mu - 1}{\mu}\right) \tag{12a, b}$$

where μ is the ductility ratio

$$\mu = \frac{\bar{\gamma}}{\gamma_e} \tag{13}$$

Finally, taking ω equal to the fundamental frequency and $\bar{\gamma}$ as the target deformation leads to the following estimate for C_H in terms of Q_y for an individual damper

$$C_H = \left[\frac{4}{\pi\omega_1\bar{\gamma}}\left(\frac{\mu - 1}{\mu}\right)\right] Q_y \tag{14}$$

Next, we need to relate C_H to an equivalent modal damping ratio.

The equations of motion for the discretized model are written as

$$\mathbf{M}\ddot{\mathbf{U}} + \mathbf{C}\dot{\mathbf{U}} + \mathbf{K}\mathbf{U} + \mathbf{P}_H = -\mathbf{M}\mathbf{E}a_g \tag{15}$$

where $\mathbf{U}$ contains the nodal translation (relative) and rotation variables; $\mathbf{M}$, $\mathbf{K}$, $\mathbf{C}$ = mass, elastic stiffness, and viscous damping matrices for the primary structure; $\mathbf{P}_H$ = nodal force vector corresponding to the hysteretic dampers; $\mathbf{E}$ defines the nodal inertia force location; a_g = ground acceleration; and dot superscripts indicate differentiation with respect to time. If $\mathbf{C}$ is taken proportional to $\mathbf{K}$

$$\mathbf{C} = \beta\mathbf{K} \tag{16}$$

the modal damping ratios for the primary structure are given by

$$\xi_i = \frac{\beta}{2}\omega_i \ (i = 1, 2, \ldots) \tag{17}$$

Eq. (17) suggests that one take C_H proportional to the transverse shear stiffness D_T

$$C_H = \beta_H D_T \tag{18}$$

With this choice, Q_y has the same spatial variation as D_T

$$D_T = \bar{D}_T[\tilde{D}_T/\tilde{D}_T(0)]; \quad Q_y = \bar{Q}_y[\tilde{D}_T/\tilde{D}_T(0)] \tag{19a,b}$$

where $\tilde{D}_T$ is defined in (2) and (6), and $\bar{D}_T$ and $\bar{Q}_y$ denote the values of D_T and Q_y at $x = 0$. The estimated equivalent modal damping ratio is given by

$$\xi_H^* = \frac{\beta_H}{2}\omega_1 = \frac{2}{\pi}\left(\frac{\mu - 1}{\mu}\right)\frac{\bar{Q}_y}{\bar{D}_T\bar{\gamma}} \tag{20}$$

Eq. (20) can be expanded further by noting that $\bar{D}_T\bar{\gamma}$ is the base shear $Q(0)$. Considering only the first mode and noting (3) leads to

$$Q(0) = \bar{D}_T\gamma = e_1 S_v W \tag{21}$$

where

TABLE 3. Seismic Criteria

Earthquake category (1)	Equivalent velocity V_E (2)	Shear deformation design criteria (3)
medium	0.75 m/s	1/400
large	1.5 m/s	1/200
extreme	3 m/s	1/100

TABLE 4. Range of Response Parameters Based on Approximate Analytical Model

S_v (m/s) (1)	μ (2)	$(\bar{\gamma})_{av}$ (3)	e_3 (4)	ξ_H^* for $\bar{Q}_y/W$ range 1% (5)	2% (6)	4% (7)
0.61	2.07	0.00207	5.66	0.0566	0.1132	0.2264
1.22	4.14	0.00414	4.17	0.0417	0.0834	0.1668
2.44	8.27	0.00827	2.42	0.0242	0.0484	0.0968

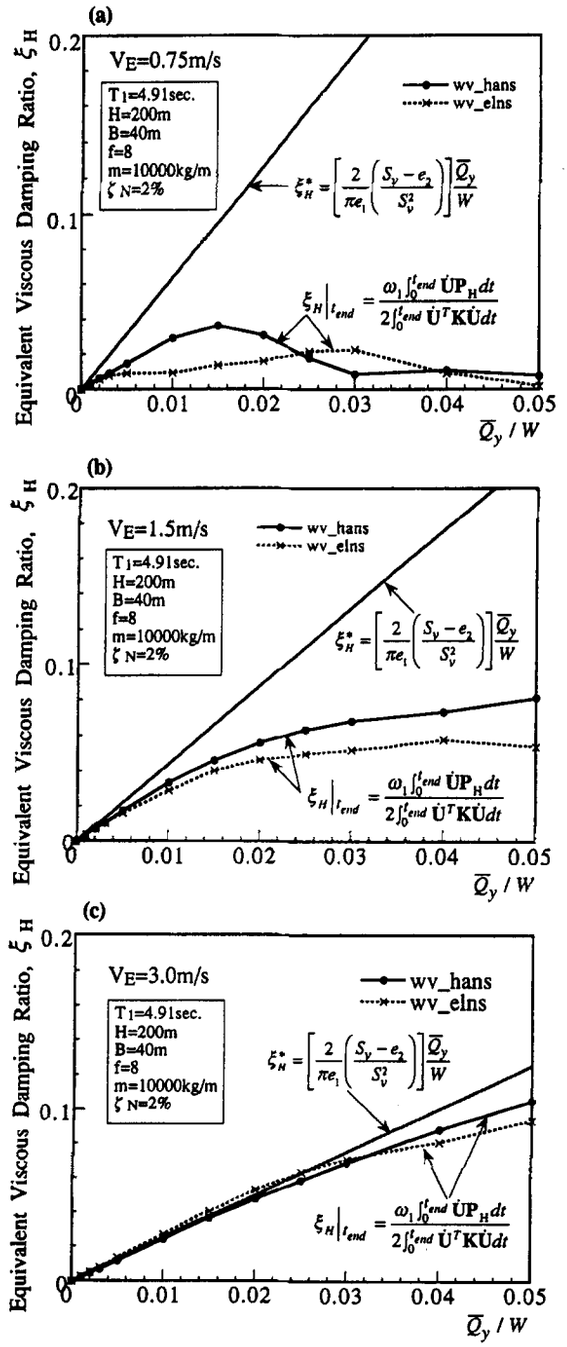

FIG. 9. Equivalent Viscous Damping Ratio versus Yield Force Level: (a) Medium Earthquake; (b) Large Earthquake; (c) Extreme Earthquake

$$e_1 = \frac{\pi}{gT_1}\left(1 + \frac{A}{3}\right)^2 \frac{1}{2/3 + A/2 + A^2/10} \tag{22}$$

S_v = spectral velocity corresponding to (T_1, ξ_1); and W = total building weight. Eq. (21) provides an estimate for the "average" shear deformation in terms of S_v and the shear rigidity at the base

$$\bar{\gamma} \approx \frac{e_1}{\bar{D}_T} S_v W \tag{23}$$

Eq. (23) only applies for small damping, say $\xi \sim 1$ to 2%. With (23) one can estimate the ductility ratio μ

$$\mu = \frac{\bar{\gamma}}{\gamma_e}\left[\frac{e_1 W}{\bar{D}_T \gamma_e}\right] S_v = \frac{S_v}{e_2} \tag{24}$$

Finally, (20) takes the form

$$\xi_H^* = \left[\frac{2}{\pi e_1}\left(\frac{S_v - e_2}{S_v^2}\right)\right]\frac{\bar{Q}_y}{W} = e_3 \frac{\bar{Q}_y}{W} \tag{25}$$

Eq. (25) is useful for generating an estimate of ξ_H^* for a particular choice of $\bar{Q}_y$ and S_v. One limitation, however, is that it is only applicable to "small" damping ratios since, as S_v tends to decrease for high damping, ξ_H^* becomes a nonlinear function of $\bar{Q}_y/W$. Numerical results illustrating this behavior are presented in the next section.

An improved estimate for the equivalent hysteretic damping ratio can be obtained by evaluating the work done by the actual hysteretic damper and an equivalent viscous damper over the duration of the earthquake. The work terms follow from (15)

$$W_H = \int_0^t \dot{\mathbf{U}}^T \mathbf{P}_H \, dt; \quad W_V = \int_0^t \dot{\mathbf{U}}^T C_H \dot{\mathbf{U}}_H \, dt; \quad W_{eq} = \int_0^t \dot{\mathbf{U}}^T \mathbf{M} \mathbf{E} a_g \, dt \tag{26a,b,c}$$

where $\mathbf{C}_H$ = equivalent viscous damping matrix. Taking

$$\mathbf{C}_H = \beta_H \mathbf{K}; \quad \beta_H = \frac{2}{\omega_1}\xi_H \tag{27a,b}$$

equating W_H to W_V, and solving for ξ_H leads to

$$\xi_H = \frac{\omega_1}{2}\frac{\int_0^t \dot{\mathbf{U}}^T \mathbf{P}_H \, dt}{\int_0^t \dot{\mathbf{U}}^T \mathbf{K} \dot{\mathbf{U}} \, dt} \tag{28}$$

Eq. (28) is used to generate the time history of the equivalent viscous damping ratio. Other useful variables are the ratios of the energy dissipated to the input energy for viscous and hysteretic damping

$$R_V = \frac{W_V}{W_{eq}}; \quad R_H = \frac{W_H}{W_{eq}} \tag{29a,b}$$

Tracking R_V and R_H over time provides a measure of the phasing between the energy input and the energy dissipated.

PARAMETRIC STUDY—EXAMPLE BUILDING

An extensive set of numerical simulations were carried out on a lumped parameter model (10 masses) of the building

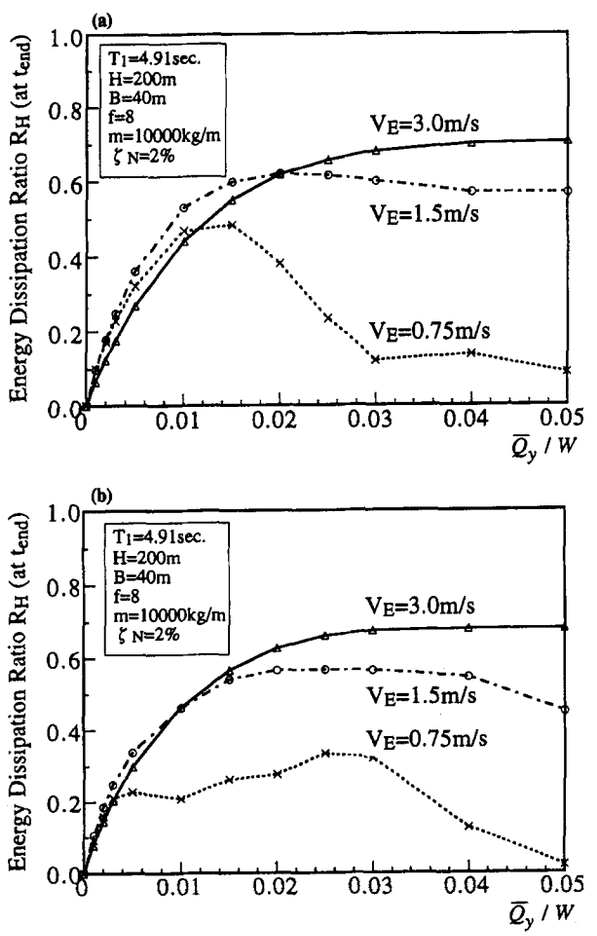

FIG. 10. Hysteric Energy Dissipation Ratio versus Yield Force Level: (a) wv_hans ground motion; (b) wv_elns ground motion

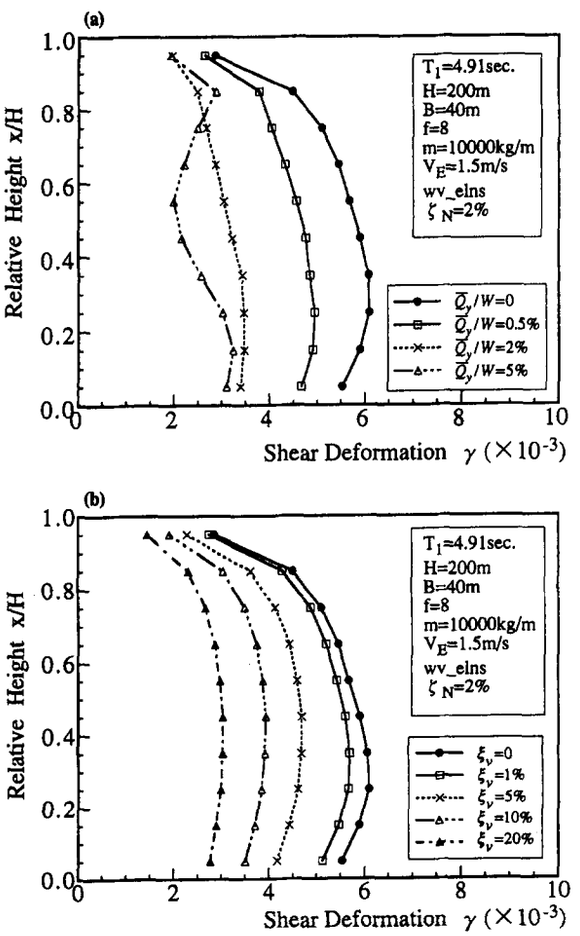

FIG. 11. Maximum Shear Deformation Profiles: (a) Hysteric Damping (Large Earthquake wv_elns); (b) Viscous Damping (Large Earthquake wv_elns)

defined earlier. Time history responses were generated using two artificial ground motions scaled such that their respective equivalent velocities are equal. Details of the scaling process are given in Huang (1994). Table 3 summarizes the relevant seismic data. Of particular interest were the amplitude and shape of the profiles for maximum deformation, and the relationship between the damper force ratio $\bar{Q}_y/W$ and the equivalent hysteretic damping ratio ξ_H. Each profile is characterized in terms of its "average" and "standard deviation" generated with time history analysis using the scaled accelerograms. The time history of the energy ratios W_V, W_H, and ξ_H^* were also evaluated. Different seismic intensity levels were considered in order to assess the influence of loading intensity on the hysteretic damping capacity as measured by the equivalent damping ratio.

The following is a list of the magnitudes of the various coefficients corresponding to this building geometry and a yield stress level of 100 MPa for the hysteretic damper brace element:

$\bar{D}_T = 5.51 \times 10^5$ kN
$\sigma_y = 100$ MPa
$\gamma_e = 10^{-3}$
$e_1 = 0.095$
$e_2 = 0.338$

The specialized forms of (23)–(25) are

$$(\bar{\gamma})_{av} = \frac{S_v(m/s)}{296}; \quad \mu = 10^3(\bar{\gamma})_{av} \tag{30a,b}$$

$$\xi_H^* = \frac{\bar{Q}_y}{W}\left\{\frac{S_v - 0.296}{0.149S_v^2}\right\} \equiv e_3\frac{\bar{Q}_y}{W} \tag{30c}$$

Table 4 summarizes the results corresponding to medium, large, and extreme loading.

The variation of the equivalent viscous damping ratio with different levels of earthquake excitation and yield force is illustrated in Fig. 9. For large earthquakes, an equivalent damping ratio of approximately 6% can be achieved with a reasonable yield force level. As expected, hysteretic damping is not as effective for medium level seismic excitation, and is essentially fully effective for extreme seismic excitation. The hysteretic energy dissipation ratio, plotted in Fig. 10, exhibits a similar pattern. This trend does not occur for viscous damping of a linear system since R_v is independent of the level of excitation in this case.

Deformation profiles corresponding to various levels of hysteretic and viscous damping for a particular earthquake are plotted in Fig. 11. There is a substantial reduction in amplitude with increased damping. To measure this effect in a more quantitative way, the mean and standard deviation were determined for each profile and are plotted versus their corresponding damping ratios in Figs. 12 and 13. Although the accelerograms are scaled to the same equivalent velocity, the deformation profiles they generate are quite different. This finding suggests that the spectral velocity is not sufficient to fully characterize an accelerogram.

Given the relationship between mean deformation, damping, and a target deformation γ^*, one can adjust the initial stiffness distribution to allow for the beneficial effect of damping. For

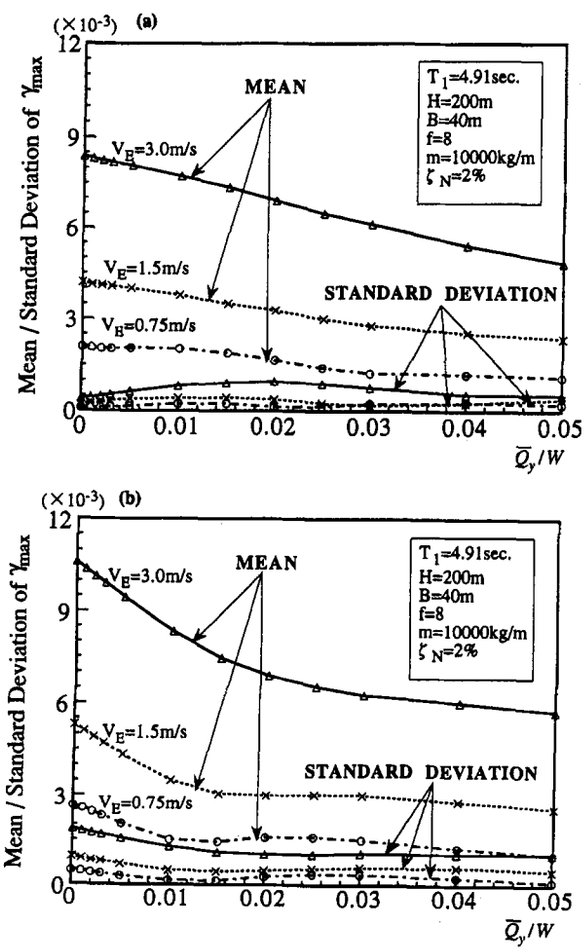

FIG. 12. Mean/Standard Deviation of Shear Deformation versus Yield Force Level: (a) wv_hans ground motion; (b) wv_eins ground motion

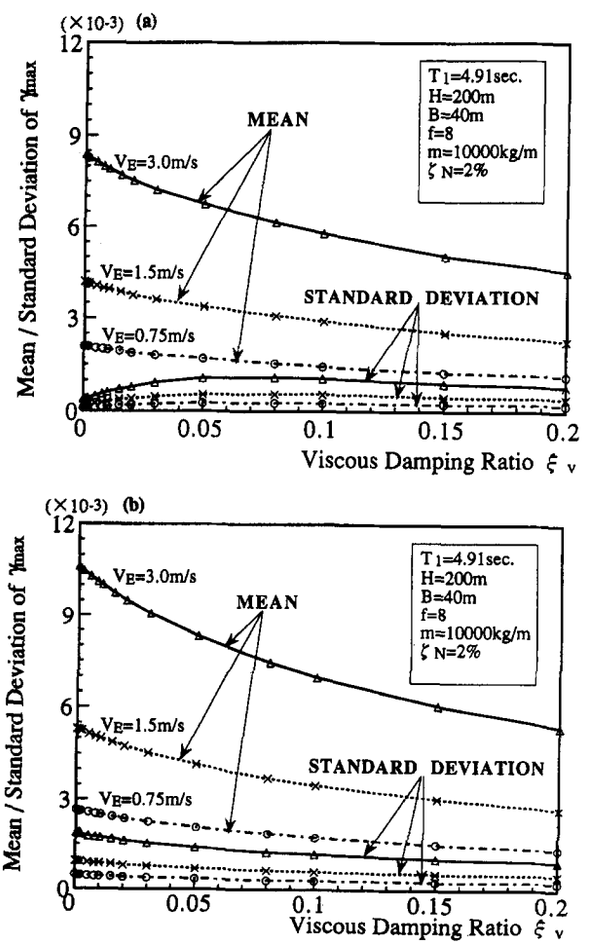

FIG. 13. Mean/Standard Deviation of Shear Deformation versus Viscous Damping Ratio: (a) wv_hans ground motion; (b) wv_eins ground motion

example, with 5% damping, the stiffness can be decreased by 20%, and still achieve the target deformation.

CONCLUSIONS

This study demonstrates that by adjusting the distribution of stiffness and hysteretic damping it is possible to control the seismic response of a building. An optimal stiffness distribution is proposed and applied to a broad set of building cases. Also, design guidelines for the magnitude and variation of the hysteretic damper properties throughout the height of the building are established and verified through numerical simulation. The results show that an effective damping ratio in the neighborhood of 5% can be obtained with a brace yield force distribution having a maximum value of 1–2% of the total building weight, and varying over the height in the same way as the stiffness. Additional numerical studies are needed to establish a robust design procedure. However, the data generated here demonstrates that a damage-control design paradigm is a realistic design approach for tall structures located in seismically active regions.

APPENDIX I. REFERENCES

Akiyama, H. (1985). *Earthquake-resistant limit-state design for buildings*. University of Tokyo Press, Tokyo, Japan.

Architectural Institute of Japan (AIJ). (1993). "Recommendation for the design of base isolated buildings." Tokyo, Japan.

Connor, J. J., and Klink, B. (1994). "Hybrid structural control." *Proc., BOSS '94 Conf.*, MIT Press, Cambridge, Mass.

Connor, J. J., and Wada, A. (1992). "Performance based design methodology for structures." *Proc., Int. Workshop on Recent Devel. in Base-Isolation Techniques for Build.*, Arch. Inst. of Japan, Tokyo, Japan, 57–70.

Huang, Y. H. (1994). "Damage controlled seismic design for tall steel buildings," PhD thesis, Tokyo Inst. of Technol., Tokyo, Japan.

Huang, Y. H., and Wada, A. (1993). "Influence of hysteretic dampers on the seismic response of high-rise buildings." *Proc., 16th Symp. on Comp. Technol. of Information, Sys. and Applications*, Arch. Inst. of Japan, Osaka, Japan, 109–114.

Iwata, M. (1994). "Damage level control design." *Arch. Inst. of Japan*, Tokyo, Japan, 109(1352), 42–44.

Iwata, M., Wada, A., Kawai, H., and Watanabe, A. (1992). "Study of damage tolerant structure: (Part 1)—study of damage tolerant design." *Summaries of technical papers of annual meeting*, Arch. Inst. of Japan, Tokyo, Japan, 1355–1356.

Tajimi, H. (1965). *Introduction to structural dynamics*. Corona Publishing Co., Ltd., Tokyo, Japan.

Wada, A., and Huang, Y. H. (1993). "Study on the optimum stiffness distribution for high-rise buildings." *Proc., 17th Symp. of Earthquake Engrg. and Appl. Earth Sci.*, Tokyo Inst. of Technol., Yokohama, Japan, 11–12.

Wada, A., Connor, J. J., Kawai, H., Iwata, M., and Watanabe, A. (1992). "Damage tolerant structures." *Proc., 5th U.S.-Japan Workshop on the Improvement of Build. Struct. Des. and Constr. Practices, ATC-15*, Appl. Technol. Council.

APPENDIX II. NOTATION

The following symbols are used in this paper:

A = parameter ($=2H/fB$);
A_b = brace cross-sectional area;
$A_g(t)$ = artificial ground acceleration;
a_g = ground acceleration;
a_i = amplitude component correspondent to the ith frequency;
B = width of building;
C_H = equivalent viscous damping parameter;
$\mathbf{C}$ = damping matrix;
$\mathbf{C}_H$ = equivalent viscous damping matrix;
D_B = bending stiffness of primary structure;
D_T = shear stiffness of the primary structure;
$\bar{D}_T$ = shear stiffness at $x = 0$;
$\tilde{D}_T$ = dimensionless shear stiffness distribution;
$\tilde{D}_B$ = dimensionless bending stiffness distribution;
$\mathbf{E}$ = nodal inertia force location matrix;
E_{HD} = energy dissipated by hysteretic dampers;
e = elongation of individual brace;
e_1 = coefficient;
e_2 = coefficient;
e_3 = coefficient;
F = brace force;
F_y = brace yield force;
f = ratio of specified shear to column strain;
g = gravitational acceleration (=980 cm/s^2);
H = total height of building;
h = story height;
$\mathbf{K}$ = elastic stiffness matrix;
k = stiffness of individual brace;
k_D = stiffness of bracing system;
k_m = stiffness of elastic bending spring;
k_q = stiffness of elastic shear spring;
$\mathbf{M}$ = mass matrix;
M = bending moment;
$M_{\max}$ = maximum bending moment obtained by SRSS method;
m = mass per unit height of building;
n_b = number of brace elements;
$\mathbf{P}_H$ = modal force vector corresponding to hysteretic dampers;
Q = shear force;
$Q_{(0)}$ = base shear force;
Q_y = yield shear force of bracing system;
$\bar{Q}_y$ = yield shear force at $x = 0$;
$Q_{\max}$ = maximum shear force obtained by SRSS method;
R = correlation coefficient in least-squares method;
R_H = ratio of energy dissipated by hysteretic damper to earthquake energy input;
R_V = ratio of energy dissipated by viscous damper to earthquake;
S_v = pseudo spectral velocity;
T = vibration period;
T_1 = fundamental period;
$\hat{T}_1$ = approximate fundamental period;
t = time;
t_{end} = time at end of earthquake;
$\mathbf{U}$ = displacement vector including translation and rotation terms;
V_E = equivalent velocity of earthquake;
W = total weight of buildings;
W_H = work done by hysteretic dampers;
W_V = work done by viscous dampers;
W_{eq} = work done by earthquake ground motion;
x = vertical coordinate;
$\tilde{x}$ = dimensionless vertical coordinate;
α = inclination angle of brace;
$\alpha_0, \alpha_1, \alpha_2, \alpha_3$ = coefficients of optimal shear stiffness distribution;
β = coefficient relating stiffens and damping;
$\beta_0, \beta_1, \beta_2, \beta_3, \beta_4$ = coefficients of optimal bending stiffness distribution;
β_H = coefficient relating stiffens and equivalent damping;
Γ_1 = participation factor for first mode;
γ = shear deformation;
$\bar{\gamma}$ = constant shear deformation;
$(\bar{\gamma})_{av}$ = average shear deformation;
γ_e = elastic limit of shear deformation;
γ^* = target shear deformation;
δ = interstory shear displacement;
$\gamma_{\max}$ = maximum shear deformation obtained by SRSS method;
ε = column strain;

ε_y^b = yield strain of brace material;
ε^* = target column strain ($\varepsilon^* = \gamma^*/f$);
ε_{max} = maximum column strain obtained by SRSS method;
θ = bending deformation angle;
κ = bending curvature;
μ = ductility ratio of brace material;
ξ = damping ratio;
ξ_i = damping ratio corresponding to ith mode;
ξ_N = natural damping ratio;
ξ_H = equivalent viscous damping ratio based on energy balance;
ξ_H^* = equivalent modal damping ratio based considering only first mode;
ξ_V = viscous damping ratio;
σ_y^b = yield stress of brace material;
φ_i = phase angle of artificial ground motion;
ω_i = circular frequency corresponding to ith mode; and
ω_1 = first circular frequency.